Biogeosciences Open Access
Discussions
EGU

Physical constraints for respiration in microbial hotspots in soil and their importance for denitrification

Steffen Schlüter[1] , Jan Zawallich[2], Hans-Jörg Vogel[1], Peter Dörsch[3]

[1] Department Soil System Sciences, Helmholtz-Centre for Environmental Research - UFZ,
5   Theodor-Lieser-Str. 4, 06120 Halle, Germany

[2] Institute of Mathematics, TU Clausthal, Erzweg 3, Clausthal-Zellerfeld, Germany

[3] Faculty of Environmental Sciences and Natural Resource Management, Norwegian University
of Life Sciences, NMBU, Aas, Norway

correspondence to: Steffen Schlüter (steffen.schlueter@ufz.de)

10   **Abstract** Soil denitrification is the most important terrestrial process returning reactive nitrogen
to the atmosphere, but remains poorly understood. In upland soils, denitrification occurs in
hotspots of enhanced microbial activity, even under well-aerated conditions, and causes harmful
emissions of nitric (NO) and nitrous oxide (N_2O). Timing and magnitude of such emissions are
difficult to predict due to the delicate balance of oxygen (O_2) consumption and diffusion in soil.

15   To study how spatial distribution of hotspots affects O_2 exchange and denitrification, we
embedded porous glass beads inoculated with either *Agrobacterium tumefaciens* (a denitrifier
lacking N_2O reductase) or *Paracoccus denitrificans* (a "complete" denitrifier) in different
architectures (random vs. layered) in sterile sand adjusted to different water saturations (30%,
60%, 90%) and measured gas kinetics (O_2, CO_2, NO, N_2O and N_2) at high temporal resolution.

20   Air connectivity, air distance and air tortuosity were determined by X-ray tomography after the
experiment. The hotspot architecture exerted strong control on microbial growth and timing of
denitrification at low and intermediate saturations, because the separation distance between the
microbial hotspots governed local oxygen supply. Electron flow diverted to denitrification in

anoxic hotspot centers was low (2-7%) but increased markedly (17-27%) at high water saturation.

25 X-ray analysis revealed that the air phase around most of the hotspots remained connected to the headspace even at 90% saturation, suggesting that the threshold response of denitrification to soil moisture could be ascribed solely to increasing tortuosity of air-filled pores. Our findings suggest that denitrification and its gaseous product stoichiometry do not only depend on the amount of microbial hotspots in aerated soil, but also on their spatial distribution. We demonstrate that

30 combining measurements of microbial activity with quantitative analysis of diffusion lengths using X-ray tomography provides unprecedented insights into physical constraints regulating soil microbial respiration in general and denitrification in particular. This opens new avenues to use observable soil structural attributes to predict denitrification and to parameterize models. Further experiments with natural soil structure, carbon substrates and microbial communities are required

35 to demonstrate this under realistic conditions.

1. Introduction

Soil carbon and nitrogen turnover is governed by soil heterogeneity at the microscale. Much of the turnover is concentrated in microsites, providing favorable conditions (pO_2, temperature, pH) and substrates (carbon, nutrients) for soil microbial activity. The partitioning of aerobic and

40 anaerobic respiration in microsites is largely controlled by the water content in the soil matrix which defines the scale across which O_2 diffuses towards microsites of high O_2-consuming activity. Aqueous diffusion lengths range from distances across thin water films in well-aerated soils, to individual soil aggregates of different radii at field capacity, up to the distance to the soil surface when the soil is saturated (Smith et al., 2003; Elberling et al., 2011; Ball, 2013; Parkin,

45 1987). Aerobic respiration is less affected by soil moisture than anaerobic respiration and typically peaks around water saturations of 20-60% in forest, grass and cropland soils (Schaufler

et al., 2010; Ruser et al., 2006; Moyano et al., 2012). Bulk soil respiration starts to decline at higher saturations due to the development of anoxic microsites with lower redox potential, supporting carbon mineralization at typically only a tenth of the rates observed under oxic

50   conditions (Keiluweit et al., 2017). Denitrification, i.e. the dissimilatory respiration of N oxyanions instead of oxygen, is commonly observed at water saturations above 60-70% and peaks beyond 90% (Ruser et al., 2006; Linn and Doran, 1984). The occurrence of anaerobic microsites is governed by the balance between saturation-dependent diffusion and microbial consumption of O_2, which in turn depends on the quantity, quality and distribution of soil organic

55   matter in the soil matrix terms and environmental factors like temperature and pH, which control microbial activity (Tecon and Or, 2017; Nunan, 2017; Smith et al., 2003). In fact, water films around decaying plant material may suffice to induce anaerobic respiration, if microbial respiration exceeds O_2 diffusion through that minute barrier (Parkin, 1987; Kravchenko et al., 2017).

60   The interplay between physical constraints and biological activity in soil controls microbial respiration at microscopic scales and complicates the prediction of denitrification and N-gas fluxes at larger scales. For instance, nitrous oxide (N_2O) emissions show notoriously large spatial variability, which has been attributed to heterogeneous distribution of anoxic microsites in the soil (Mathieu et al., 2006; Röver et al., 1999; Parkin, 1987; Parry et al., 1999). Together with the

65   often observed high temporal variability of microbial respiration and its fluctuations under transient conditions, this has led to the notion of "hotspots" and "hot moments" for microbial activity and emissions (Groffman et al., 2009; Kuzyakov and Blagodatskaya, 2015). "Hotspots" of denitrification have traditionally been linked to diffusion constraints in soil aggregates. Cell numbers and O_2 concentration have been shown to decline exponentially towards aggregate

70   centers (Sexstone et al., 1985; Horn et al., 1994; Zausig et al., 1993; Højberg et al., 1994) and the

critical aggregate radius for the development of anoxic centers and is typically >1 mm (Sierra and

Renault, 1996; Højberg et al., 1994; Schlüter et al., 2018), However, anoxic microsites have also

been reported for smaller aggregates (equivalent diameter of 0.03-0.13 mm) in well-aerated,

repacked soils (Keiluweit et al., 2018).

75   An important, but often neglected aspect of physical diffusion constraints on microbial

respiration is the spatial distribution of microbial hotspots within the soil matrix. Incubation

experiments were either designed to control the aggregate size in repacked soil (Mangalassery et

al., 2013; Miller et al., 2009) or the volume fraction of sieved soil mixed evenly into sterile quartz

sand (Keiluweit et al., 2018). Some incubation studies were carried out with undisturbed soil and

80   investigated diffusion constraints within the pore network (Rabot et al., 2015). However, these

studies did not address the location of hotspots nor the diffusion lengths towards air-filled pores.

The vast majority of incubations studies merely reports bulk soil properties like carbon and

nitrogen content, bulk density and water saturation. Notable exceptions are Kravchenko et al.

(2017) who controlled the position of microbial hotspots by placing decaying plant leaf material

85   into repacked soils with different aggregate sizes and water saturations and Ebrahimi and Or

(2018), who placed several layers of remolded aggregates as artificial hotspots into a sand matrix

and controlled the volume fraction of anaerobic and aerobic respiration by adjusting the water

table in the sand column. Such systematic studies with simplified soil analogues, yet fully

accounting for transport processes from and towards hotspots, including interactions between

90   hotspots, are needed to improve our understanding about how physical constraints on microbial

respiration control the anaerobic soil volume and transient denitrification activity.

The objective of the present study was to study the interplay between microbial activity and physical diffusion in controlling aerobic and anaerobic respiration for different spatial distributions of hotspots. We embedded uniform artificial hotspots inoculated with denitrifying

95   pure cultures (Schlüter et al., 2018) in sterile sand, which was adjusted to different water saturations. We hypothesized that the competition for oxygen would depend on the separation distance between the hotspots, which in turn would control microbial cell growth and O_2 consumption and thus affect the timing of the aerobe-anaerobe transition in respiration, i.e. the onset of denitrification. Further, by placing hotspots inoculated with complete (*P. denitrificans*)

100   and truncated (*A. tumefaciens*) denitrifiers in distinct horizontal layers, we expected to see interactions with respect to overall N_2O turnover. To capture the highly dynamic respiration kinetics, we monitored O_2, CO_2, NO, N_2O and N_2 exchange between the headspace and the sand-hotspot matrix at high temporal resolution. The morphology of the air-filled pore space in terms of air connectivity, air tortuosity and air distance was determined by X-ray computed tomography

105   after the experiment.

2. Material and methods

2.1.   Microbial hotspots

Two facultative anaerobic bacteria were used in this study. *Paracoccus denitrificans* expresses all denitrification enzymes necessary to reduce NO_3^- to N_2, whereas *Agrobacterium tumefaciens*

110   lacks the gene *nos*Z encoding nitrous oxide reductase (N_2OR), which makes N_2O the final denitrification product. Moreover, the two strai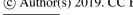ns differ in their regulatory phenotypes with respect to inducing denitrification in response to oxygen depletion, which leads to characteristic patterns of product accumulation (Bergaust et al., 2011). *P. denitrificans* induces NO and N_2O

5

reductase early during O_2 depletion (Bergaust et al., 2010), thus releasing little N_2O. By contrast,

115   *A. tumefaciens* is known to be less stringent in controlling intermediates which may result in the

release of large amounts of NO, up to cell-toxic, milli-molar concentrations (Bergaust et al.,

2008). Both strains were grown in Sistrom's medium (Sistrom, 1960) as described in a previous

study (Schlüter et al., 2018), but at double strength to provide enough substrate for depleting O_2

during aerobic growth. The medium was amended with 10 mM NH_4NO_3 and 5 mM KNO_3 for

120   anaerobic growth. To produce microbial hotspots, porous borosilicate glass beads (VitraPOR

P100, ROBU Glasfilter Geräte GmbH) with a diameter of 7 mm, a porosity of 32% and a

medium pore diameter of 60 µm were saturated with freshly inoculated growth medium ($\approx 10^8$

cells ml^{-1}) by submersion into one of the two cultures. In the following, the inoculated porous

glass beads are referred to as *At-* (*A. tumefaciens*) and *Pd-* (*P. denitrificans*) hotspots. Detailed

125   information about the culture conditions and the inoculation procedure can be found in Schlüter

et al. (2018).

2.2.   Repacked sand

Fifty *At* and *Pd* hotspots each were placed into 120 ml of washed, sterile quartz sand (0.2-0.5 mm

grain size) yielding a volume fraction of 14% (20 ml; Fig. S1a). The sand was packed into 240

130   ml glass jars (Ball Corporation, Bloomfield, CA) in portions of 10 ml layers and adjusted to

target saturation by adding sterile water with a spray can. The packing procedure resulted in some

minor changes in porosity between layers and some larger gaps around the hotspots (Fig. S3)

which affected air distribution in the sand (Fig. S2a). Three saturations were used, corresponding

to water-filled pore spaces (WFPS) of 30, 60 and 90%. The fully saturated hotspots were placed

135   into the sand at three different architectures (**Figure 1**). For the "random" distribution, the

hotspots were placed in five equidistant (~9.8 mm, center to center) horizontal layers with a

random distribution of ten *At* and ten *Pd* hotspots per layer. For the "layered *At/Pd*" and "layered *Pd/At*" distributions, all fifty hotspots of each strain were placed into one of two horizontal layers spaced 21 mm from each other (center to center) at an average headspace distance of 18.2 and

140   39.2 mm, respectively, where the order represents *top/bottom*. Care was taken to keep the hotspots cool (on crushed ice) during the packing procedure. The pore size distribution of the porous hotspots and the sand in the bulk soil and in hotspot vicinity are reported in Figure S3.

2.3.   Incubation

To establish aerobic and anaerobic growth patterns and denitrification kinetics for both bacterial

145   strains when growing inside the glass beads, a pre-experiment was conducted without sand. Fifty *Pd* or *At* hotspots were placed in empty 120 ml serum bottles (Fig. S1b) and incubated at 15°C under either oxic (He/O$_2$ 80/20%) or anoxic (He 100%) conditions in two replicates per treatment. Headspace concentrations of O$_2$, CO$_2$, NO, N$_2$O and N$_2$ were measured every 4 h by piercing the septum with a hypodermic needle mounted to the robotic arm of an autosampler

150   (GC-PAL, CTC Analytics, Switzerland). The autosampler was connected to a gas chromatograph (Agilent Model 7890A, Santa Clara, CA, USA) and a NO analyzer (Teledyne 200. San Diego, CA, USA) via a peristaltic pump. Detailed information about the robotized incubation system and the experimental setup can be retrieved elsewhere (Molstad et al., 2007; Schlüter et al., 2018).

In the main experiment, freshly inoculated glass beads were packed into incubation vessels as

155   described above, three replicates for each of the nine combinations of saturation and hotspot distribution. Jars with 30% and 60% WFPS were flushed with He/O$_2$ for 40 min, using ten cycles of vacuum (3 min) and purging (1 min). Jars with 90% WFPS were flushed using 180 cycles of mild vacuum (~ 600 mbar) and O$_2$/He purging to avoid structural changes of the packed columns

160   due to bubbling of trapped gas. The jars were then placed into a water bath kept at 15°C and after

temperature equilibration O_2/He overpressure was released. Gas concentrations in the headspace

were analyzed as described above. Gas production and consumption kinetics were used to

calculate the fraction of electrons diverted to O_2 or N oxyanions and thus to estimate the

contribution of denitrification to total respiration (e^-_{denit}/e^-_{total}) (Schlüter et al., 2018; Bergaust

et al., 2011). The NO/(NO+ N_2O + N_2) and N_2O/(NO+ N_2O + N_2) product ratios were estimated

165   from the cumulative release of gaseous denitrification products (NO, N_2O, N_2), after subtracting

precursors from products (NO from N_2O + N_2 and NO + N_2O from N_2). The rationale behind the

latter was to mimic an open system, in which N-gases released to the atmosphere are not

available any longer as electron acceptors for denitrification. Details about the calculation of

denitrification product ratios can be found in the Supporting Information (SI 1.2).

170   ## 2.4.   X-ray tomography and image analysis

After the incubation experiment, the glass jars were scanned with X-ray micro-tomography (X-

tek XCT 225, Nikon Metrology) with a beam energy of 145 kV, a beam current of 280 µA, an

exposure time of 708 ms per frame, a 0.5 mm copper filter for reducing beam hardening artefacts

and a total of 3000 projection for a full scan. Individual hotspots were also scanned (100 kV,

175   90µA, 1000ms per frame, no filter) to analyze the internal pore morphology. The 2D projections

were reconstructed into a 3D image with a resolution of 35 µm using a filtered-back projection

algorithm in the X-tek CT Pro 3D software. Image processing from raw gray-scale data (**Figure

1a**) to segmented data including sand grains, air and water (**Figure 1b-c**) was carried out

according to well-established protocols for multi-phase segmentation (Schlüter et al., 2014). The

180   porous glass beads were assigned to *At* or *Pd* hotspots according to the orientation of the flat end

in the random architecture or by the vertical position in the layered architecture (**Figure 1b-c**).

The segmented images were analyzed with respect to three different spatial attributes of the air-filled pore spaces deemed important for oxygen supply. 1. Air connectivity by distinguishing isolated air-filled pores and air-filled pores with a continuous path to the headspace (yellow and

185   red in **Figure 1d**). Air connectivity is then defined as the ratio of connected air-filled pore space and total air-filled pore space 2. Air tortuosity as derived from the geodesic length of connected air-filled pores. The geodesic length is the distance of any connected air voxel to the headspace along curved paths around obstacles like solid particles and water-blocked pores **(Fig. 1e)**. Air tortuosity is the ratio between geodesic and vertical Euclidean distance to the headspace averaged

190   over all connected, air-filled voxels. It is a proxy for the diffusive transport of gaseous oxygen in air-filled pores 3. Air distances of water-filled pores as defined by the average geodesic distance from any water voxel to the closest air-filled pore with headspace connection (white in **Fig. 1f**). Air distance is a proxy for the slow diffusive transport of dissolved oxygen. All image processing steps were carried out with Fiji/ImageJ (Schindelin et al., 2012) and associated plugins (Legland

195   et al., 2016; Doube et al., 2010) or with VG Studio Max 2.1 (Volume Graphics). Each image processing and analysis step is explained in detail in the supporting information (SI 1.3).

[Figure 1]

3. Results

3.1.   Aerobic respiration and denitrification in unconstrained

200   **hotspots without sand**

At grew faster than *Pd* at 15°C in the experiment with loosely placed porous glass beads as indicated by faster O_2 consumption and CO_2 accumulation in the oxic treatment (**Figure 2a,b**). Also under fully anoxic conditions, *At* accumulated CO_2 faster than *Pd* (Figure 2b). N-gas

kinetics clearly reflected the distinct regulatory phenotypes of the two bacterial denitrifiers.

205   Anoxic *At* instantly accumulated a large amounts of NO (**Figure 2c**) which persisted until all

NO$_3^-$ was reduced to N$_2$O (as judged from the stable plateau in N$_2$O, **Figure 2d**). Due to slower

growth and O$_2$ consumption, *Pd* induced denitrification much later than *At*, but accumulated less

intermediates (NO, N$_2$O) than *At*. Oxically incubated *Pd* accumulated no detectable NO,

indicating efficient regulation of denitrification when switched slowly to anaerobic conditions in

210   hotspots. Also, NO may have been reduced to N$_2$O when diffusing from the anoxic center to the

boundary of the hotspot. In the initially oxic treatments, denitrification contributed 7% to the total

electron flow in *At* hotspots and 13% in *Pd* hotspots, reflecting the fact that (i) *Pd* has one more

reduction step in the denitrification sequence and that (ii) *At* used less nitrate for anaerobic

respiration in anoxic hotspots centers and more oxygen for aerobic respiration in oxic hotspots

215   margins than *Pd*.

[Figure 2]

3.2.   Effects of hotspot distribution in sand

The distribution of microbial hotspots within the sand strongly impacted bulk respiration. This is

evident for treatments with medium saturation (60% WFPS) for the first 210 h of incubation

220   (**Figure 3**) and with other saturations for the entire incubation period (300 h; Figures S4-6). The

random distribution of hotspots allowed for much faster aerobic growth than the layered

architectures, leading to complete consumption of O$_2$ from the jars after 70 h (**Figure 3a**). Given

the slow growth of *Pd* (**Figure 2a**), initial O$_2$ consumption was dominated by the activity of *At*

hotspots turning them partly anoxic. Hence, the pronounced NO peak in the random treatment,

225   coinciding with complete O$_2$ exhaustion from the headspace (**Figure 3c**), was due to *At* activity,

Biogeosciences
Discussions

similar to what was seen in the unconstrained *At* hotspots under anoxic conditions (**Figure 2c**). N$_2$O production was observed long before O$_2$ was depleted from the headspace (**Figure 3d**) and is attributed entirely to *At* denitrification. *Pd* denitrification did not start before all O$_2$ was depleted and manifested itself in a transient increase in N$_2$O production at ~70 h together with an

230   exponential increase in N$_2$ production (**Figure 3e**) which was also observed with unconstrained *Pd* hotspots (**Figure 2e**). Note that the apparent net consumption of CO$_2$ (**Figure 3b**) upon O$_2$ depletion was due to internal alkalization driven by accelerating denitrification, once all hotspots turned anoxic.

[Figure 3]

235   In the layered architectures, O$_2$ consumption was slower and complete anoxia was not reached before 120 h into the incubation. In contrast to the random architecture, less O$_2$ was available for each individual hotspot in the densely packed hotspot layers, allowing for less aerobic growth per unit time. As a consequence, there was more time for fully denitrifying *At* hotspots to interact with *Pd* hotspots which induced denitrification gradually between 80 and 120 h. Indeed, less N$_2$O

240   accumulated in the headspace than in the random treatment (**Figure 3d**, S6d) and the onset of N$_2$ accumulation appeared long before complete O$_2$ depletion from the headspace (**Figure 3a,e**). In other words, *Pd* hotspots consumed N$_2$O produced in *At* hotspots. Upon O$_2$ depletion in the headspace, a burst of NO production occurred (**Figure 3c**) as seen previously with *At* hotspots (**Figure 2c**). However, since *Pd* denitrification was now fully developed, the NO peak was much

245   more short-lived than with the random distribution, because *Pd* hotspots reduced NO produced by *At* hotspots all the way to N$_2$.

The effect of vertical order in the layered hotspot architecture was small, but consistent among all denitrification products. The distribution with *Pd* hotspots on top (layered *Pd/At*) consumed the

NO and N_2O produced in *At* hotspots much quicker than the *At/Pd* architecture (**Figure 3c-d**) and

250   accumulated N_2 faster after complete O_2 depletion (**Figure 3e**). Both observations highlight the

effect of shorter diffusion distances between the headspace and the *Pd* hotspot layer in the

layered *Pd/At* architecture.

3.3.   Effects of matrix saturation

Differences in water saturation resulted in different absolute amounts of oxygen initially present

255   in the jars (**Figure 4a**) but did not affect the O_2 concentration in the sand matrix. Oxygen was

depleted slightly faster at 60% than at 90% saturation even though there was absolutely more O_2

initially present at 60% WFPS. This illustrates the paramount role of oxic growth for the oxic-

anoxic transition in the hotspots: the more O_2 available initially, the stronger the aerobic growth

and the faster the oxic-anoxic transition.

260   Increasing saturation from 60 to 90% in the randomly distributed hotspots had a strong effect on

the timing and accumulation of denitrification products. The expected NO burst upon O_2

depletion was damped by two orders of magnitude (**Figure 4c**), because the oxic-anoxic

transition proceeded more smoothly in the 90% treatment and NO was reduced further to N_2O

before it could escape to the headspace. On the other hand, N_2O and N_2 production commenced

265   earlier in the 90% than in the 60% treatment (**Figure 4d-e**), indicating that O_2 availability was *a

priori* smaller irrespective of metabolic activity (which was larger in the 60% treatment). The

switch from net N_2O production to net N_2O consumption indicates the moment when microbial

activity in *Pd* hotspots caught up with *At* hotspots.

[Figure 4]

270   Surprisingly, O_2 consumption in the 30% treatments was slow despite having the largest amount

of O_2 in the jar. This was caused by unintended substrate limitation. Due to overlapping pore size

distribution between porous hotspots and sand (Fig. S3c), medium was sucked by capillary force

from the hotspot into the surrounding sand, as could be seen in a parallel experiment with

brilliant blue dye (Fig. S7). This separated cells, which were likely immobilized in the pore space

275   of the hotspots, temporarily from a considerable fraction of the carbon and NO_3^- supplied with the

medium, before the dissolved substrate would diffuse back into the hotspots due to the evolving

gradient induced by consumption in the hotspots. Decreasing the saturation from 60% to 30%

also resulted in different timing and accumulation of denitrification products. The slow oxic

growth of both *At* and *Pd* hotspots due to the substrate diffusion limitation at 30% WFPS

280   provided more time for *Pd* hotspots to interact with *At* hotspots than in the 60% WFPS treatment.

Indeed, the NO burst from *At* hotspots after complete O_2 exhaustion in the random architecture

was 50% higher at 30% WFPS indicating higher *At* cell numbers due to prolonged oxic growth

(**Figure 4c, Figure 5c**), whereas the N_2O peak was 50% lower, due to concomitant N_2O

reduction in *Pt* hotspots (**Figure 4d , Figure 5d**).

285   ## 3.4.   Mass balances

By the end of the incubation, oxygen was exhausted in all treatments. Likewise, NO_3^- was

consumed by all treatments, except for the layered hotspots at 30% and 60% WFPS. This means

that respiration was electron acceptor limited and that the cumulated recovery of denitrification

products can be compared with the amount of NO_3^- initially present (Figure S8). The balance

290   between aerobic and anaerobic respiration, e_{denit}^-/e_{total}^- (Bergaust et al., 2011), is given by the

electron flow to nitrogenous electron acceptors relative to the total electron flow, including O_2

respiration (**Figure 5**). When seen over all three water saturations, early stage denitrification

under oxic headspace conditions (**Figure 5a**) showed a threshold response to increasing moisture

with disproportionally higher e^-_{denit}/e^-_{total} ratios at 90% WFPS (17-27%) than at 60% or 30%.

295 The proportions of electrons diverted to denitrification at low and medium saturations were small

(2-7%) and even smaller than those observed in unconstrained hotspots (7-13%). Differences

between saturations were less pronounced when the entire incubation period is considered

(**Figure 5b**), since fully anoxic conditions during late stage incubation overrode saturation

effects. Overall, the effect of hotspot architecture on e^-_{denit}/e^-_{total} ratios was smaller than the

300 effect of saturation.

This stands in stark contrast to the pronounced effect of hotspot architecture on denitrification

product ratios (**Figure 5c, d**). Hotspot architecture governed growth rates through local

competition for O_2 and therewith the number of active cells involved in net production sites (*At*

hotspots) and net consumption sites (*Pd* hotspots) of NO once O_2 was exhausted. In layered

305 hotspot architectures there was hardly any net-release of NO to the headspace irrespective of

saturation (**Figure 5c**). With random hotspot architecture, there was substantial NO release, the

magnitude of which, however, decreased linearly with saturation. This pattern in NO

stoichiometry clearly reflects the number of *At* cells at the moment of complete O_2 depletion, as

affected by oxic growth which lasted longer with lower saturation. The N_2O product ratio

310 (**Figure 5d**) was influenced by both saturation and hotspot architecture. In layered architectures,

the N_2O ratio increased exponentially with increasing saturation similar to what was observed for

relative electron flow to denitrification (**Figure 5a**). In random architectures, the N_2O product
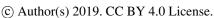
ratio was consistently higher than in layered architectures irrespective of saturation, yet the

highest ratio was reached at 60% WFPS, due to the most vigorous growth, and hence fastest oxic-

315 anoxic transition at intermediate saturation.

Biogeosciences

Discussions

[Figure 5]

3.5.   Pore space properties

At the lowest saturation (30% WFPS), the entire air-filled pore space was connected to the

headspace (**Figure 6a**) and tortuosity was close to unity, i.e. the diffusion lengths in air only

320   depended on the vertical distance to the headspace (**Figure 6b**). The diffusion distances in water-

filled pores (**Figure 6c**) corresponded to the size of small, evenly distributed water clusters. At

medium saturation (60% WFPS), the amount of disconnected air was still negligible and

tortuosity only slightly increased. The increase in air distance was due to a few large water

pockets, which were caused by the step-wise addition of water to the repacked sand. Only at 90%

325   saturation a considerable air volume of 5-20% became disconnected from the headspace. The

path along which the remaining air was connected to the headspace became more tortuous with

increasing saturation and average diffusion distances in water to the connected air cluster

increased to 1 mm. This is still surprisingly short as compared to the size of the hotspots (7 mm).

Independent tests showed that the high air connectivity at this low air content was facilitated by

330   vacuum application during He/O_2-purging prior to the incubation. Directly after packing, the

continuous air cluster only reached 10-15 mm into the sand (data not shown), whereas bubbling

due to vacuum application formed continuous air channels that reached deep into the sand matrix

connecting even the deepest hotspots with the headspace. Moreover, some larger gaps remained

around hotspots during packing which tended to be air-filled after wetting. This is reflected in the

335   consistently higher air-connectivity, lower air tortuosity and lower air distance, when only pores

in the direct vicinity of hotspots are analyzed (**Figure 6a-c**). More than 90% of hotspot surfaces

still had a direct air-filled connection with the headspace at 90% WFPS (**Figure 6a**). Depth

profiles of these pore space attributes are reported in Fig. S2.

[Figure 6]

340   **4. Discussion**

4.1.   Physical constraints on denitrification kinetics

The experimental setup in this incubation study was designed to investigate physical constraints
on microbial respiration in hotspots as affected by the interplay between gaseous diffusion
through a sterile matrix and local competition for oxygen. For this, we compared different
345   combinations of water saturation in the matrix and spatial distributions of hotspots. The setup is a
coarse simplification of soil in which metabolic activity in hotspots not only depends on oxygen
supply, but also on diffusion of substrates from the matrix to the hotspots. As such, our
experiment does not allow to draw direct conclusions about the functioning of hotspots in real
soils with respect to denitrification and its product stoichiometry. However, by placing
350   denitrifiers and their substrates into hotspots, we considerably reduced the level of complexity
and created a system that is amenable to studying the dynamic interrelations between denitrifier
growth, oxygen consumption and induction of denitrification by gas kinetics. Soil N_2O emissions
are known to be highly variable in time and a unifying concept incorporating dynamic changes in
denitrification activity and product stoichiometry in response to changing environmental
355   conditions is still missing. Our model system provides a first data set for validating mathematical
process models that are explicit for structural distribution of hotspots and dynamic changes in
boundary conditions (here mimicked by different hotspot architectures and declining oxygen
concentrations in the headspace of batch incubations, respectively). The development of such
models is a core activity of the DASIM project (http://www.dasim.net/). By combining metabolic

16

Biogeosciences
Discussions

360   measurements with advanced structural imaging and computation, we also provide a link to

parameterizing such models with real soil data in future research.

Inoculating growing denitrifiers into porous glass beads and embedding them in sterile sand

resulted in a highly dynamic system with respect to oxygen consumption and induction of

denitrification. This was intended for the sake of experimental depth, but it must be noted that

365   oxic-anoxic transitions are likely slower, i.e. less dynamic in real-soil hotspots. In real soils, even

highly organic hotspots contain a fair amount of recalcitrant organic C that limits microbial

growth and oxygen consumption. Also with respect to denitrification stoichiometry, real soils

may be expected to be less dynamic as multiple denitrifying phenotypes contained in the natural

soil microbiome (Roco et al., 2017) utilize denitrification intermediates mutually.

370   Notwithstanding, soil NO and N_2O emissions are known to be episodic in nature. Large,

denitrification driven emission pulses occur upon abrupt changes in O_2 availability, caused by

external factors like heavy rainfalls or soil freezing (Flessa et al., 1995), O_2 consumption by

nitrification after ammoniacal fertilization (Huang et al., 2014) or incorporation of easily

degradable organic matter (Flessa et al., 1995) which cannot be captured satisfactorily by

375   common steady-state models for soil respiration and N_2O emission (Parton et al., 2001; Li et al.,

1992). Even though the concept of hotspots is central in the understanding of denitrification

dynamics in upland soils, common soil denitrification models do not account for the dynamics of

spatially explicit hotspots in the soil matrix but rather scale bulk denitrification with a generic

anoxic volume fraction (Li et al., 2000; Blagodatsky et al., 2011). To advance soil denitrification

380   models, it is obvious that microbial respiration dynamics in hotspots have to be targeted, both

conceptually (Wang et al., 2019) and experimentally (Kravchenko et al., 2017; Ebrahimi and Or,

2018). Our study is a first step in this direction.

One of the main findings of this study is that soil microbial respiration and the propensity to develop denitrifying anoxic hotspots does depend on their distribution in space. The onset of

385   denitrification and its kinetics was linked to the spatial and temporal extent of anoxia developing in hotspot centers, which was governed by the interplay between denitrifier growth and diffusion constraints and hotspot architecture had a strong impact on this interplay. When distributed randomly, microbial activity was most disperse relative to available oxygen, resulting in more growth, faster O_2 draw down and earlier anoxia than when packed densely in layers (**Figure 3**).

390   Rapid oxic-anoxic transition led to higher release rates of denitrification intermediates increasing the product ratios of NO and N_2O (**Figure 5c-d**). This effect was most pronounced at low and intermediate saturations but was dampened at 90%WPFS because oxygen supply was impeded by bulk diffusion irrespective of hotspot placement. Thus, our results highlight the significance of hotspot distribution at low soil moistures and exemplifies why N_2O emissions are notoriously

395   difficult to predict under these conditions.

Even though we failed to fully synchronize *At* and *Pd* growth in time, our experiment demonstrates that contrasting denitrification phenotypes may interact in modulating N_2O flux to the atmosphere. *Pd* hotspots reduced N_2O released from *At* hotspots irrespective of the layers' orientation (**Figure 3d**), which can be attributed to the high degree of air connectivity in the sand

400   column (**Figure 1d**). We had expected more N_2O reduction with *Pd* on top (layered *Pd/At*), but since *At* grew faster than *Pd*, partial anoxia and NO and N_2O formation was induced in *At*, long before N_2O consuming activity was induced in *Pd* hotspots. Future experiments with artificial hotspots should therefore carefully consider potential growth rates and air connectivity in packed soil.

Biogeosciences
Discussions

4.2.   Physical constraints on cumulative denitrification

The cumulative release of gaseous denitrification products, as described by electron flow ratios, depended less on hotspot architecture than on soil moisture. Electron flows to denitrification ranged from <5% of total respiratory flow at low to medium saturations (30, 60% WFPS) to almost 23% at 90% WFPS (**Figure 5a**). We attribute this low denitrification electron flow to the small active volume relative to the sterile sand matrix (the total volume fraction of hotspots was 14%, less of which was actually anoxic) and the large amount of oxygen initially present in the incubation jars. Yet, we found a typical, non-linear denitrification response to soil moisture (**Figure 5a**). This threshold behavior is well known (Weier et al., 1993) and has been attributed to a disproportional contribution of small pores to the anoxic volume at higher saturation (Schurgers et al., 2006). In our system, consisting of coarse sand with a relatively homogenous pore size distribution, we attribute the non-linear response to an increase in tortuosity of air-filled pores that was pronounced enough to impair the supply of hotspots with oxygen. Air connectivity and distance to the next continuous, air-filled pore also increased non-linearly, but did not reach a critical value (**Figure 6**), ruling out that differences in NO and N_2O release at different saturations were due to gas entrapment but rather due to elongated diffusion pathways in air-filled pore networks, leading to longer residence times of denitrification intermediates and stronger reduction of intermediates in hotspots along the way to the headspace. Saturation-dependent threshold behavior for denitrification is a well-studied phenomenon in soils (Linn and Doran, 1984; Ruser et al., 2006; Paul et al., 2003), but for a lack of pore scale measurements often attributed to reduced bulk soil diffusivity. In undisturbed soil, the relative importance of air connectivity and distances between air-filled and water-filled pores might be more relevant for impairing oxygen supply and inducing denitrification. Air connectivity to the headspace was shown to affect N_2O emissions in terms of intensity and speed in repeated wetting/drying cycles

in an intact soil column (Rabot et al., 2015). In agricultural soil with different crop rotations, N_2O

430 emissions were shown to correlate positively with the volume fraction of soil with macropore

distances larger than 180 µm, used as an *ad-hoc* definition for poorly aerated soil (Kravchenko et

al., 2018). In a mesocosm study on microstructural drivers for local redox conditions, none of the

investigated soil pore metrics derived from X-ray CT data (excluding those examined here)

correlated with redox kinetics during a wetting/drying cycle (Wanzek et al., 2018). Hence,

435 combining metabolic monitoring by high-resolution gas kinetics with direct assessment of

diffusion lengths of gaseous and dissolved oxygen and denitrification products via X-ray

microtomography emerges as a promising tool to study physical constraints for aerobic and

anaerobic respiration in soil. However, meaningful metrics derived from X-ray data relevant for

denitrification are yet to be developed and will require additional experiments with both artificial

440 and real soils. Improved understanding of factors and mechanisms controlling denitrification and

N gas emission on a three-dimensional micro-scale may help to design and test soil management

strategies that mediate the return of excess nitrogen to the atmosphere in a controlled way, i.e.

with as little as possible NO and N_2O release, be it by crop residue (Kravchenko et al., 2017), pH

(Russenes et al., 2016) or irrigation (Bergstermann et al., 2011) management. At the same time,

445 our experiments call for the implementation of spatially explicit reaction-diffusion algorithms

(Hron et al., 2015; Ebrahimi and Or, 2016) in soil process models. For instance, diffusion lengths

between hotspots and air-filled pores connected to the headspace may serve as useful measure to

parametrize model concepts like the anaerobic soil volume fraction in larger-scale continuum

models (Li et al., 2000; Schurgers et al., 2006; Blagodatsky et al., 2011).

Biogeosciences
Discussions

5. Conclusions

450

Using a highly simplified model system, we demonstrate that the factorial combination of water saturation and hotspot architecture creates a wealth of denitrification kinetics in response to declining oxygen concentrations with highly variable NO and N_2O release rates. Even though our experiment was conducted in a closed system, with growing denitrifier strains and a limited

455 amount of substrate, the results are relevant for real soils in that they give a worst-case scenario of population dynamics and metabolic activity in hotspots. Hotspot architecture played a more pronounced role for denitrification kinetics at lower soil moisture (30 and 60% WFPS). Hence, denitrification and its gaseous product stoichiometry do not only depend on the amount of microbial hotspots in aerated soil, but also on their spatial distribution. The total amount of

460 denitrification measured as cumulative electron flow, in turn, depended more on water saturation which is in line with the well-known saturation-dependent threshold behavior in denitrification also found in natural soil. For the case of artificial soil used in our study, we found that this threshold behavior was best explained by increased air tortuosity at high saturations. Future experiments with artificial and natural soils are needed to fully capture the regulation of

465 denitrification at the micro-scale.

6. Acknowledgments

7. References

Ball, B. C.: Soil structure and greenhouse gas emissions: a synthesis of 20 years of
475   experimentation, European Journal of Soil Science, 64, 357-373, 10.1111/ejss.12013, 2013.

Bergaust, L., Shapleigh, J., Frostegard, A., and Bakken, L.: Transcription and activities of NOx
reductases in Agrobacterium tumefaciens : The influence of nitrate, nitrite and oxygen
availability, Environ. Microbiol., 10, 3070-3081, 2008.

Bergaust, L., Mao, Y., Bakken, L., and Frostegard, A.: Denitrification response patterns during
480   the transition to anoxic respiration and posttranscriptional effects of suboptimal pH on nitrogen
oxide reductase in Paracoccus denitrificans Appl. Environ. Microbiol., 76, 6387-6396, 2010.

Bergaust, L., Bakken, Lars R., and Frostegård, Å.: Denitrification regulatory phenotype, a new
term for the characterization of denitrifying bacteria, Biochemical Society Transactions, 39, 207-
212, 10.1042/bst0390207, 2011.

485   Bergstermann, A., Cárdenas, L., Bol, R., Gilliam, L., Goulding, K., Meijide, A., Scholefield, D.,
Vallejo, A., and Well, R.: Effect of antecedent soil moisture conditions on emissions and
isotopologue distribution of N_2O during denitrification, Soil Biology and Biochemistry, 43, 240-
250, https://doi.org/10.1016/j.soilbio.2010.10.003, 2011.

Blagodatsky, S., Grote, R., Kiese, R., Werner, C., and Butterbach-Bahl, K.: Modelling of
490   microbial carbon and nitrogen turnover in soil with special emphasis on N-trace gases emission,
Plant and Soil, 346, 297, 10.1007/s11104-011-0821-z, 2011.

Doube, M., Kłosowski, M. M., Arganda-Carreras, I., Cordelières, F. P., Dougherty, R. P.,
Jackson, J. S., Schmid, B., Hutchinson, J. R., and Shefelbine, S. J.: BoneJ: Free and extensible
bone image analysis in ImageJ, Bone, 47, 1076-1079, 2010.

495   Ebrahimi, A., and Or, D.: Microbial community dynamics in soil aggregates shape
biogeochemical gas fluxes from soil profiles - upscaling an aggregate biophysical model, Global
Change Biology, 22, 3141-3156, 2016.

Ebrahimi, A., and Or, D.: Dynamics of soil biogeochemical gas emissions shaped by remolded
aggregate sizes and carbon configurations under hydration cycles, Global Change Biology, 24,
500   e378-e392, 10.1111/gcb.13938, 2018.

Elberling, B., Askaer, L., Jørgensen, C. J., Joensen, H. P., Kühl, M., Glud, R. N., and Lauritsen,
F. R.: Linking Soil O_2, CO_2, and CH_4 Concentrations in a Wetland Soil: Implications for CO_2
and CH_4 Fluxes, Environmental Science & Technology, 45, 3393-3399, 10.1021/es103540k,
2011.

505   Flessa, H., Dörsch, P., and Beese, F.: Seasonal variation of N2O and CH4 fluxes in differently
managed arable soils in southern Germany, Journal of Geophysical Research: Atmospheres, 100,
23115-23124, doi:10.1029/95JD02270, 1995.

Groffman, P. M., Butterbach-Bahl, K., Fulweiler, R. W., Gold, A. J., Morse, J. L., Stander, E. K., Tague, C., Tonitto, C., and Vidon, P.: Challenges to incorporating spatially and temporally
510 explicit phenomena (hotspots and hot moments) in denitrification models, Biogeochemistry, 93, 49-77, 2009.

Højberg, O., Revsbech, N. P., and Tiedje, J. M.: Denitrification in soil aggregates analyzed with microsensors for nitrous oxide and oxygen, Soil Science Society of America Journal, 58, 1691-1698, 1994.

515 Horn, R., Stepniewski, W., Wlodarczyk, T., Walenzik, G., and Eckhardt, F.: Denitrification rate and microbial distribution within homogeneous model soil aggregates, Int. Agrophysics, 8, 65-74, 1994.

Hron, P., Jost, D., Bastian, P., Gallert, C., Winter, J., and Ippisch, O.: Application of Reactive Transport Modeling to Growth and Transport of Microorganisms in the Capillary Fringe, Vadose
520 Zone Journal, 14, 10.2136/vzj2014.07.0092, 2015.

Huang, T., Gao, B., Hu, X.-K., Lu, X., Well, R., Christie, P., Bakken, L. R., and Ju, X.-T.: Ammonia-oxidation as an engine to generate nitrous oxide in an intensively managed calcareous Fluvo-aquic soil, Scientific Reports, 4, 3950, 10.1038/srep03950, 2014.

Keiluweit, M., Wanzek, T., Kleber, M., Nico, P., and Fendorf, S.: Anaerobic microsites have an
525 unaccounted role in soil carbon stabilization, Nature Communications, 8, 1771, 10.1038/s41467-017-01406-6, 2017.

Keiluweit, M., Gee, K., Denney, A., and Fendorf, S.: Anoxic microsites in upland soils dominantly controlled by clay content, Soil Biology and Biochemistry, 118, 42-50, https://doi.org/10.1016/j.soilbio.2017.12.002, 2018.

530 Kravchenko, A. N., Toosi, E. R., Guber, A. K., Ostrom, N. E., Yu, J., Azeem, K., Rivers, M. L., and Robertson, G. P.: Hotspots of soil N2O emission enhanced through water absorption by plant residue, Nature Geoscience, 10, 496, 10.1038/ngeo2963, 2017.

Kravchenko, A. N., Guber, A. K., Quigley, M. Y., Koestel, J., Gandhi, H., and Ostrom, N. E.: X-ray computed tomography to predict soil N2O production via bacterial denitrification and N2O
535 emission in contrasting bioenergy cropping systems, GCB Bioenergy, 0, doi:10.1111/gcbb.12552, 2018.

Kuzyakov, Y., and Blagodatskaya, E.: Microbial hotspots and hot moments in soil: Concept & review, Soil Biology and Biochemistry, 83, 184-199, 2015.

Legland, D., Arganda-Carreras, I., and Andrey, P.: MorphoLibJ: integrated library and plugins
540 for mathematical morphology with ImageJ, Bioinformatics, 32, 3532-3534, 2016.

Li, C., Frolking, S., and Frolking, T. A.: A model of nitrous oxide evolution from soil driven by rainfall events: 1. Model structure and sensitivity, Journal of Geophysical Research: Atmospheres, 97, 9759-9776, doi:10.1029/92JD00509, 1992.

545   Li, C., Aber, J., Stange, F., Butterbach-Bahl, K., and Papen, H.: A process-oriented model of N2O and NO emissions from forest soils: 1. Model development, Journal of Geophysical Research: Atmospheres, 105, 4369-4384, 2000.

Linn, D., and Doran, J.: Effect of water-filled pore space on carbon dioxide and nitrous oxide production in tilled and nontilled soils, Soil Science Society of America Journal, 48, 1267-1272, 1984.

550   Mangalassery, S., Sjögersten, S., Sparkes, D. L., Sturrock, C. J., and Mooney, S. J.: The effect of soil aggregate size on pore structure and its consequence on emission of greenhouse gases, Soil and Tillage Research, 132, 39-46, https://doi.org/10.1016/j.still.2013.05.003, 2013.

Mathieu, O., Lévêque, J., Hénault, C., Milloux, M.-J., Bizouard, F., and Andreux, F.: Emissions and spatial variability of N_2O, N_2 and nitrous oxide mole fraction at the field scale, revealed with
555   15N isotopic techniques, Soil Biology and Biochemistry, 38, 941-951, 2006.

Miller, M. N., Zebarth, B. J., Dandie, C. E., Burton, D. L., Goyer, C., and Trevors, J. T.: Denitrifier Community Dynamics in Soil Aggregates under Permanent Grassland and Arable Cropping Systems, Soil Science Society of America Journal, 73, 1843-1851, 10.2136/sssaj2008.0357, 2009.

560   Molstad, L., Dörsch, P., and Bakken, L. R.: Robotized incubation system for monitoring gases (O_2, NO, N_2O, N_2) in denitrifying cultures, Journal of Microbiological Methods, 71, 202-211, 2007.

Moyano, F. E., Vasilyeva, N., Bouckaert, L., Cook, F., Craine, J., Curiel Yuste, J., Don, A., Epron, D., Formanek, P., Franzluebbers, A., Ilstedt, U., Kätterer, T., Orchard, V., Reichstein, M.,
565   Rey, A., Ruamps, L., Subke, J. A., Thomsen, I. K., and Chenu, C.: The moisture response of soil heterotrophic respiration: interaction with soil properties, Biogeosciences, 9, 1173-1182, 10.5194/bg-9-1173-2012, 2012.

Nunan, N.: The microbial habitat in soil: Scale, heterogeneity and functional consequences, Journal of Plant Nutrition and Soil Science, 180, 425-429, 10.1002/jpln.201700184, 2017.

570   Parkin, T. B.: Soil microsites as a source of denitrification variability, Soil Science Society of America Journal, 51, 1194-1199, 1987.

Parry, S., Renault, P., Chenu, C., and Lensi, R.: Denitrification in pasture and cropped soil clods as affected by pore space structure, Soil Biology and Biochemistry, 31, 493-501, https://doi.org/10.1016/S0038-0717(98)00101-1, 1999.

575   Parton, W. J., Holland, E. A., Del Grosso, S. J., Hartman, M. D., Martin, R. E., Mosier, A. R.,
      Ojima, D. S., and Schimel, D. S.: Generalized model for NO_x and N_2O emissions from soils,
      Journal of Geophysical Research: Atmospheres, 106, 17403-17419, doi:10.1029/2001JD900101,
      2001.

      Paul, K. I., Polglase, P. J., O'Connell, A. M., Carlyle, J. C., Smethurst, P. J., and Khanna, P. K.:
580   Defining the relation between soil water content and net nitrogen mineralization, European
      Journal of Soil Science, 54, 39-48, doi:10.1046/j.1365-2389.2003.00502.x, 2003.

      Rabot, E., Lacoste, M., Hénault, C., and Cousin, I.: Using X-ray Computed Tomography to
      Describe the Dynamics of Nitrous Oxide Emissions during Soil Drying, Vadose Zone Journal,
      14, 10.2136/vzj2014.12.0177, 2015.

585   Roco, C. A., Bergaust, L. L., Bakken, L. R., Yavitt, J. B., and Shapleigh, J. P.: Modularity of
      nitrogen-oxide reducing soil bacteria: linking phenotype to genotype, Environmental
      Microbiology, 19, 2507-2519, doi:10.1111/1462-2920.13250, 2017.

      Röver, M., Heinemeyer, O., Munch, J. C., and Kaiser, E.-A.: Spatial heterogeneity within the
      plough layer: high variability of N_2O emission rates, Soil Biology and Biochemistry, 31, 167-
590   173, 1999.

      Ruser, R., Flessa, H., Russow, R., Schmidt, G., Buegger, F., and Munch, J. C.: Emission of N_2O,
      N_2 and CO_2 from soil fertilized with nitrate: effect of compaction, soil moisture and rewetting,
      Soil Biology and Biochemistry, 38, 263-274, https://doi.org/10.1016/j.soilbio.2005.05.005, 2006.

      Russenes, A. L., Korsaeth, A., Bakken, L. R., and Dörsch, P.: Spatial variation in soil pH controls
595   off-season N2O emission in an agricultural soil, Soil Biology and Biochemistry, 99, 36-46,
      https://doi.org/10.1016/j.soilbio.2016.04.019, 2016.

      Schaufler, G., Kitzler, B., Schindlbacher, A., Skiba, U., Sutton, M. A., and Zechmeister-
      Boltenstern, S.: Greenhouse gas emissions from European soils under different land use: effects
      of soil moisture and temperature, European Journal of Soil Science, 61, 683-696, 10.1111/j.1365-
600   2389.2010.01277.x, 2010.

      Schindelin, J., Arganda-Carreras, I., Frise, E., Kaynig, V., Longair, M., Pietzsch, T., Preibisch,
      S., Rueden, C., Saalfeld, S., and Schmid, B.: Fiji: an open-source platform for biological-image
      analysis, Nature methods, 9, 676-682, 2012.

      Schlüter, S., Sheppard, A., Brown, K., and Wildenschild, D.: Image processing of multiphase
605   images obtained via X-ray microtomography: A review, Water Resources Research, 50, 3615-
      3639, 2014.

      Schlüter, S., Henjes, S., Zawallich, J., Bergaust, L., Horn, M., Ippisch, O., Vogel, H.-J., and
      Dörsch, P.: Denitrification in Soil Aggregate Analogues-Effect of Aggregate Size and Oxygen
      Diffusion, Frontiers in Environmental Science, 6, 10.3389/fenvs.2018.00017, 2018.

610   Schurgers, G., Dorsch, P., Bakken, L., Leffelaar, P., and Haugen, L. E.: Modelling soil
       anaerobiosis from water retention characteristics and soil respiration, Soil Biology &
       Biochemistry, 38, 2637-2644, 10.1016/j.soilbio.2006.04.016, 2006.

       Sexstone, A. J., Revsbech, N. P., Parkin, T. B., and Tiedje, J. M.: Direct measurement of oxygen
       profiles and denitrification rates in soil aggregates, Soil science society of America journal, 49,
615   645-651, 1985.

       Sierra, J., and Renault, P.: Respiratory Activity and Oxygen Distribution in Natural Aggregates in
       Relation to Anaerobiosis, Soil Science Society of America Journal, 60, 1428-1438,
       10.2136/sssaj1996.03615995006000050020x, 1996.

       Sistrom, W. R.: A Requirement for Sodium in the Growth of Rhodopseudomonas spheroides,
620   Microbiology, 22, 778-785, 1960.

       Smith, K. A., Ball, T., Conen, F., Dobbie, K. E., Massheder, J., and Rey, A.: Exchange of
       greenhouse gases between soil and atmosphere: interactions of soil physical factors and
       biological processes, European Journal of Soil Science, 54, 779-791, 10.1046/j.1351-
       0754.2003.0567.x, 2003.

625   Tecon, R., and Or, D.: Biophysical processes supporting the diversity of microbial life in soil,
       FEMS Microbiology Reviews, 41, 599-623, 10.1093/femsre/fux039, 2017.

       Wang, B., Brewer, P. E., Shugart, H. H., Lerdau, M. T., and Allison, S. D.: Soil aggregates as
       biogeochemical reactors and implications for soil–atmosphere exchange of greenhouse gases—A
       concept, Global Change Biology, doi:10.1111/gcb.14515, 2019.

630   Wanzek, T., Keiluweit, M., Varga, T., Lindsley, A., Nico, P. S., Fendorf, S., and Kleber, M.: The
       Ability of Soil Pore Network Metrics to Predict Redox Dynamics is Scale Dependent, Soil
       Systems, 2, 66, 2018.

       Weier, K. L., Doran, J. W., Power, J. F., and Walters, D. T.: Denitrification and the
       Dinitrogen/Nitrous Oxide Ratio as Affected by Soil Water, Available Carbon, and Nitrate, Soil
635   Science Society of America Journal, 57, 66-72, 10.2136/sssaj1993.03615995005700010013x,
       1993.

       Zausig, J., Stepniewski, W., and Horn, R.: Oxygen Concentration and Redox Potential Gradients
       in Unsaturated Model Soil Aggregates, Soil Science Society of America Journal, 57, 908-916,
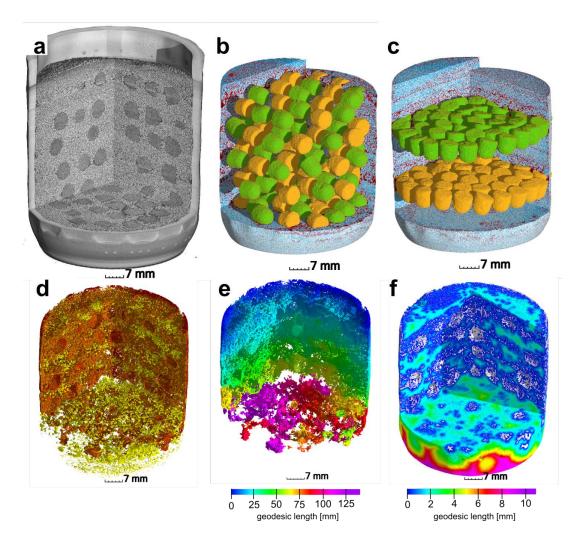   10.2136/sssaj1993.03615995005700040005x, 1993.

640

Figure 1. Upper panel: (a) X-ray CT scan of an incubation jar with random hotspot architecture and medium saturation (60% WFPS). (b) Image segmentation of the same jar into air (red), water (blue), sand (transparent), *A. tumefaciens* hotspots (orange) and *P. denitrificans* hotspots (green). (c) A different jar at medium saturation (60% WFPS) with layered *Pd/At* hotspot architecture. Lower panel: a jar with random distribution at high saturation (90% WFPS). (d) Air connectivity, determined as the volume fraction of air connected to the headspace (red, disconnected air shown in yellow). (e) Air tortuosity as derived from the geodesic length to the headspace within the connected air cluster. (f) Diffusion lengths determined as the geodesic length to the closest connected air cluster (white) within water-filled pores.
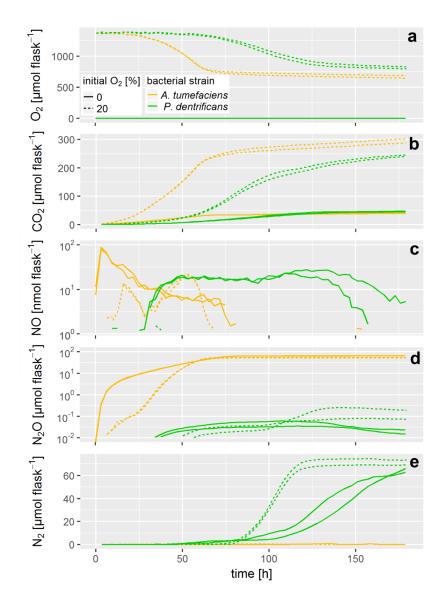
645

650 **Figure 2: Gas kinetics of individual sets of hotspots inoculated with two different bacterial strains, under oxic and anoxic conditions: (a) O_2, (b) CO_2, (c) NO, (d) N_2O, (e) N_2. Note the logarithmic ordinate in (c) and (d).**
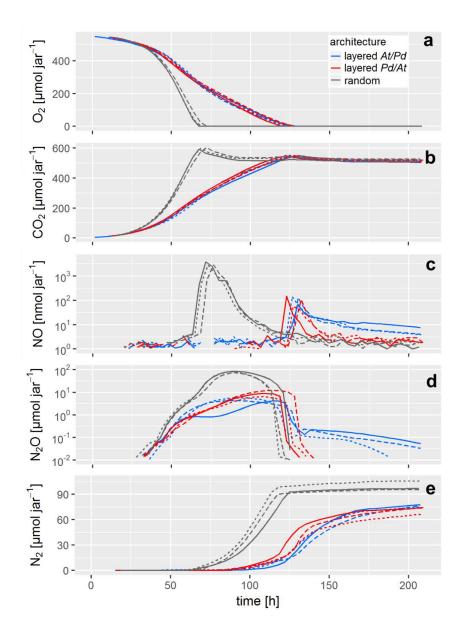
Figure 3: Gas kinetics in all treatments at medium saturation (60% WFPS) for three different hotspot architectures: (a)
O_2, (b) CO_2, (c) NO, (d) N_2O, (e) N_2. Note the logarithmic ordinate in (c) and (d). Different lines styles represent replicates.
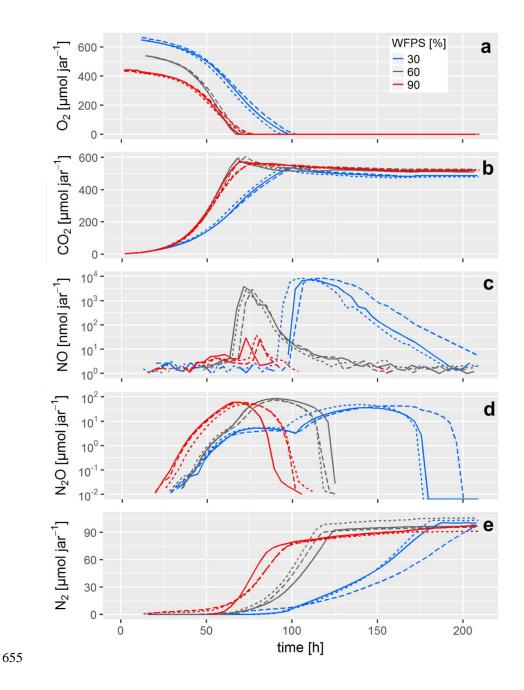
Figure 4: Gas kinetics of randomly placed hotspots at three different saturations: (a) O_2, (b) CO_2, (c) NO, (d) N_2O, (e) N_2. Note the logarithmic ordinate in (c) and (d). Different lines styles represent replicates.
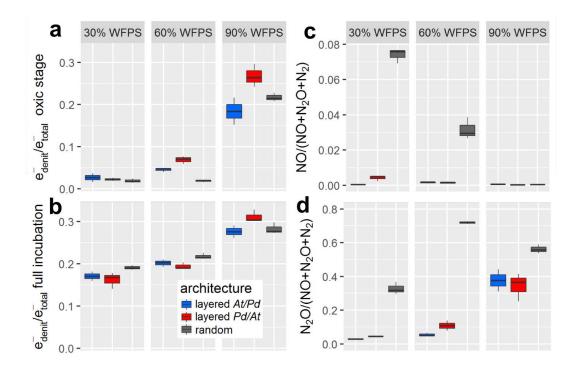
655

Figure 5: The proportion of denitrification in total respiration expressed as relative electron flow for all architectures and saturations. Values are reported for (a) the initial, oxic to hypoxic stage (O$_2$ present in headspace) and (b) for the full incubation period of 300 h. The product ratios for NO (c) and N$_2$O (d) consider the full incubation period and are corrected for the release of precursor gases. Data shown as box-whisker plots: Whiskers- min-max, middle lines - median.
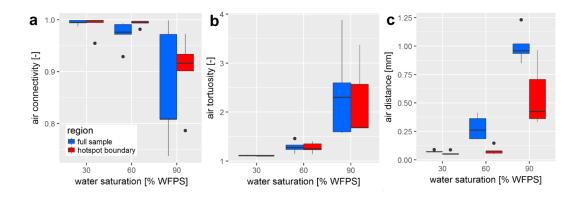

Figure 6: Morphological properties of air-filled pores at different saturations averaged over different hotspots architectures (n=5). These properties are reported separately for the entire pore space within the region of interest (full sample) and for the pore space in direct vicinity to the porous glass beads (hotspot boundary): (a) air connectivity represents the volume fraction of air with direct connection to the headspace. (b) Air tortuosity represents the ratio between geodesic length to the headspace and Euclidean distance for any voxel within the connected air-cluster. (c) Air distance represents the geodesic distance to the connected air cluster within the water-filled pores. Data shown as box-whisker plots: Whiskers- min-max, middle lines – median, dots: outliers.